Kinetic Analyses Reveal Multiple Steps in Forming TonB−FhuA Complexes from *Escherichia coli*†

Cezar M. Khursigara,‡ Gregory De Crescenzo,§ Peter D. Pawelek,‡ and James W. Coulton*,‡

Department of Microbiology and Immunology, McGill University, 3775 University Street, Montreal, Quebec, Canada H3A 2B4 and Protein−Protein Interaction Facility, Sheldon Biotechnology Centre, McGill University, 3773 University Street, Montreal, Quebec, Canada H3A 2B4

Received September 30, 2004; Revised Manuscript Received December 3, 2004

ABSTRACT: FhuA, an outer membrane receptor of *Escherichia coli*, facilitates transport of hydroxamate siderophores and siderophore−antibiotic conjugates. The cytoplasmic membrane complex TonB−ExbB−ExbD provides energy for transport via the proton motive force. This energy is transduced by protein−protein interactions between TonB and FhuA, but the molecular determinants of these interactions remain uncharacterized. Our analyses of FhuA and two recombinant TonB species by surface plasmon resonance revealed that TonB undergoes a kinetically limiting rearrangement upon initial interaction with FhuA: an intermediate TonB−FhuA complex of 1:1 stoichiometry was detected. The intermediate then recruits a second TonB protein. Addition of ferricrocin, a FhuA-specific ligand, enhanced amounts of the 2:1 complex but was not essential for its formation. To assess the role of the cork domain of FhuA in forming a 2:1 TonB−FhuA complex, we tested a FhuA deletion (residues 21−128) for its ability to interact with TonB. Analytical ultracentrifugation demonstrated that deletion of this region of the cork domain resulted in a 1:1 complex. Furthermore, the high-affinity 2:1 complex requires the N-terminal region of TonB. Together these in vitro experiments establish that TonB−FhuA interactions require sequential steps of kinetically limiting rearrangements. Additionally, domains that contribute to complex formation were identified in TonB and in FhuA.

The outer membrane (OM)[1] of Gram-negative bacteria acts as a barrier that limits the passive diffusion of large molecules through porin proteins. Molecules larger than the molecular mass exclusion limits of porins require an energy-dependent mode of transport. These transport systems are protein complexes whose components reside within the OM, periplasm, and cytoplasmic membrane (CM) (*1*). Iron, an essential element, is transported into *Escherichia coli* by iron-chelating siderophores, but its bioavailability is limited at physiological conditions due to the formation of insoluble ferric hydroxides. Siderophores are too large to diffuse passively across the OM and therefore require high-affinity receptor-mediated transport. One such high-affinity uptake system relies on FhuA, the receptor for the hydroxamate siderophore ferricrocin (Fc). FhuA also facilitates the transport of siderophore−antibiotic conjugates such as albomycin and rifamycin CGP 4832 and is the receptor for phages T5, T1, Φ80, and UC-1, for colicin M, and for the antimicrobial peptide microcin MccJ21. Energy for siderophore transport is provided by the CM complex TonB−ExbB−ExbD. This complex delivers electrochemical potential via the proton motive force of the CM and transduces energy to the OM receptor (*2*−*4*).

FhuA (*5*, *6*) and related OM receptors FepA (*7*), FecA (*8*), and BtuB (*9*) share common structural features. Each is comprised of two domains: an N-terminal globular cork and a 22-stranded β-barrel. The cork domain resides within the barrel, occluding the large pore of the barrel domain. To transduce energy from the CM to the OM, TonB must interact with OM receptors. The Ton box, located near the periplasmic face of each receptor, is a conserved motif proposed to be a primary site for TonB−OM receptor interactions (*1*).

Recent studies have focused on characterization of the TonB−OM receptor mechanism at the molecular level. Two key areas of interest include elucidation of the site (or sites) of TonB interaction with OM receptors and determination of the oligomeric state of TonB, either alone or in complex with different OM receptors. Initial biochemical evidence of TonB interactions with OM receptors came from in vivo cross-linking studies of TonB and FepA (*10*). Other in vivo and in vitro cross-linking studies (*11*−*13*) demonstrated that specific ligands of OM receptors enhanced association with TonB. These findings also corroborated genetic analyses that suggested a functional interaction near Gln160 of TonB (*14*).

† This research was supported by operating grants to J.W.C. from the Natural Sciences and Engineering Research Council of Canada (NSERC) and the Canadian Institutes of Health Research (CIHR).

* To whom correspondence should be addressed: Phone: (514) 398−3929. Fax: (514) 398-7052. E-mail: james.coulton@mcgill.ca.

‡ Department of Microbiology and Immunology.

§ Sheldon Biotechnology Centre.

[1] Abbreviations: Φ_{avg}, weight-averaged apparent vbar; AUC, analytical ultracentrifugation; C1, two-dimensional sensor chip; C8E4, *n*-octyltetraoxyethylene; CM, cytoplasmic membrane; CM4, carboxymethylated dextran matrix sensor chip; EDC, *N*-ethyl-*N*-(3-dimethylaminopropyl)carbodiimide-hydrochloride; Fc, ferricrocin; LDAO, lauryldimethylamine oxide; M_b, buoyant molecular mass; NHS, *N*-hydroxysuccinimide; NTA, Ni^{2+}-nitrilotriacetic; OM, outer membrane; PDEA, 2-(2-pyridinylthio)ethanolamine; RU, resonance unit(s); SPR, surface plasmon resonance.

10.1021/bi047882p CCC: $30.25
Published on Web 02/10/2005

Determination of the X-ray crystallographic structure for the C-terminal fragment of TonB (residues 164−239) published by Chang et al. (*15*) and confirmed by Koedding et al. (*16*) raised fundamental questions about the oligomeric state of TonB in the context of its interactions with OM receptors. The structures depict C-terminal TonB as a tightly intertwined dimer. The solution behavior of C-terminal TonB was analyzed by our group (*17*) and others (*16*) using analytical ultracentrifugation (AUC). These studies established that dimerization of this domain of TonB was not a crystallographic artifact. However, longer TonB constructs including TonB residues 145−239, 116−239 (*16*), and 33−239 (*17*) sediment as monomers when analyzed by AUC. Our AUC studies of TonB residues 33−239 with FhuA demonstrated a 2:1 (TonB−FhuA) complex in which the presence of the FhuA-specific ligand Fc enhanced and stabilized complex formation (*17*). Determination of 1:1 TonB−FhuA stoichiometries by gel filtration (*16*) did not include longer TonB constructs in which the N-terminal region was shown to enhance TonB−FhuA complex formation. The in vivo dimerization of TonB was also investigated (*18*) in protein hybrid experiments: the C-terminal TonB fragment (residues 164−239) was detected in vivo as a dimer, while a longer protein (residues 33−239) did not dimerize, in agreement with our in vitro findings (*17*).

Our previous surface plasmon resonance (SPR) study focused on steady-state interactions between FhuA (M_r 78, 992) and two TonB variants: (i) a C-terminal TonB fragment termed TonB (CT); residues 155−239, M_r 11 903; and (ii) a full-length TonB minus its signal/anchor sequence termed TonB (FL); residues 32−239, M_r 24 900. Because TonB requires membrane anchorage and interaction with the energy-coupling Exb proteins, these TonB variants are unable to drive active transport. Our objectives were to study isolated TonBs and by SPR define kinetic and thermodynamic parameters for TonB−FhuA interactions. To do so we expressed and purified the two TonB variants, now engineered with a single cysteine at the N-terminal linker region. The cysteine residue allowed coupling of the TonB variants in an oriented fashion, intending to reflect the in vivo orientation of TonB anchored in the CM. Using this optimized experimental design we also characterized the kinetics of interactions with full-length FhuA and a mutant FhuA harboring a deletion in its cork domain (FhuAΔ21−128; deleted residues 21−128, M_r 68 103). Our SPR results, in combination with sedimentation velocity AUC data, highlight the intricacy of TonB−FhuA complex formation in vitro.

EXPERIMENTAL PROCEDURES

Strains. *E. coli* strain AW740 harbors plasmid pHX405 and expresses recombinant FhuA with a hexahistidine tag at position 405 (*19*). *E. coli* ER2566 was transformed with pET28 plasmids expressing TonB (FL) and TonB (CT) as described previously (*17*). All plasmids were confirmed for nucleotide fidelity by DNA sequencing at Sheldon Biotechnology Centre, McGill University.

Site-Directed Mutagenesis of TonB Proteins. Site-directed mutagenesis was accomplished using the QuickChange Site-directed Mutagenesis Kit (Stratagene, #200519). Briefly, primers were designed to anneal to the linker region of the pET28 vector in order to change a glycine residue to a cysteine; codon underlined: (5′-CATCATCACAGCAGCTGC-CTGGTGCCGCGCGGC-3′ and 5′-GCCGCGCGGCACCAG-GCAGCTGCTGTGATGATG-3′). All subsequent steps were followed according to the manufacturer's guidelines.

Insertion of Hexahistidine Tag in FhuAΔ21−128. Plasmid pGCΔ21−128 encoding the FhuAΔ21−128 mutant (*20*) was doubly digested with *Sph*I and *Sal*I. The resulting fragment encoding the internally deleted *fhuA* gene was then ligated into pHX405 vector (*21, 22*) previously digested with the same enzymes. This construct corresponded to FhuAΔ21−128 mutant that is hexahistidine tagged at residue 405. The recombinant plasmid was then amplified in *E. coli* DH5α, and sequence fidelity was verified. Last, pGC405Δ21−128 was transformed into *E. coli* AW740.

Protein Purification. FhuA and FhuAΔ21−128 were extracted and purified (*19*) in *N*-lauryldimethylamine oxide (LDAO; Fluka) and detergent exchanged on Q Sepharose anion-exchange media (Amersham Bioscience) into Biacore running buffer: 100 mM HEPES (pH 7.4), 150 mM NaCl, 0.1% Tween 20 (Protein grade, Calbiochem). TonB (FL) and TonB (CT), both containing engineered cysteine residues, were purified using Ni^{2+}-nitrilotriacetic acid Superflow resin (Qiagen) followed by cation exchange with SP Sepharose (Amersham Bioscience). Prior to SPR experiments, each TonB protein was dialyzed against Biacore running buffer.

Analytical Ultracentrifugation. Samples were prepared for AUC by dialysis against 100 mM HEPES (pH 8.0), 150 mM NaCl, and 0.4% *n*-octyltetraoxyethylene (C8E4; Bachem). Proteins were concentrated to 1 mg/mL and mixed in 2:1 molar ratios (TonB (FL):FhuA(Δ21−128)) for the analysis of complexes. Ligand-loaded receptor was prepared by mixing Fc and FhuAΔ21−128 in a 10:1 molar ratio, 30 min at room temperature. Excess Fc was removed by dialysis against AUC buffer using Spectrapor dialysis membrane (POR-6, 25 kDa cutoff).

Sedimentation velocity experiments were performed using a Beckman XL-I Analytical Ultracentrifuge. The sample and reference sectors of 1.2 cm path length double-sector ultracentrifuge cells were filled with 400 μL of protein and AUC buffer, respectively. All sedimentation velocity runs were performed at 40 000 rpm with absorbance scans monitored at 280 nm in 10-min intervals over a total spin time of 4 h at 24.6 °C.

Sedimentation velocity data were analyzed using computer program SEDFIT (*23*) as previously described (*17*). Briefly, initial sedimentation profiles were obtained by fitting the data to the continuous c(S) model, allowing for estimates of initial *s* values for all sedimenting species. Buoyant molecular mass (M_b) values and refined *s* values for uncomplexed species were determined using SEDFIT's noninteracting discrete species model. Initial M_b values were obtained from the known molecular mass of each protein. Sedimentation parameters of uncomplexed species were constrained during analysis of sedimentation velocity data of heterogeneous protein mixtures. Sedimentation parameters of species corresponding to protein−protein complexes were refined using the nonlinear regression algorithms of SEDFIT. Optimization of the fits were performed by varying stoichiometric combinations of *s*1, *s*2, and *s*3 and repeating the constrained analyses until distributions of residuals were observed to be fully random and rmsd errors were minimized.

Surface Plasmon Resonance. SPR measurements were performed using Biacore 2000 and 3000 optical biosensors (Biacore, AB). The data collection rate and temperature were set to 10 Hz and 25 °C, respectively.

TonBs were immobilized on CM4 or C1 sensor chips (Biacore, AB) using thiol-coupling procedures (*24*). Surfaces were activated by injections of *N*-hydroxysuccinimide/*N*-ethyl-*N*-(3-dimethylaminopropyl)carbodiimide-hydrochloride (NHS/EDC, 25 μL) and 2-(2-pyridinylthio)ethanolamine (PDEA; dissolved in borate buffer pH 8.5, 30 μL) according to manufacturer's recommendations. TonB (FL) or TonB (CT) diluted in 10 mM acetate buffer (pH 4.5) were individually coupled to different surfaces by manual injection at 5 μL/min (final concentrations: 160 nM for TonB (FL) and 145 nM for TonB (CT)) until the desired amounts of protein were immobilized. Deactivation of remaining activated groups was accomplished by injection of L-cysteine solution dissolved in 0.1 M formate buffer (pH 4.3; 35 μL). Control surfaces were prepared using the same procedure, injecting buffer rather than TonB proteins. Before conducting any experiments, TonB surfaces were conditioned by buffer injections followed by two 50 μL pulses of 5 mM NaOH, 0.1% Tween 20, and an EXTRACLEAN procedure (flow rate set at 100 μL/min). The conditioning cycle was repeated four times.

Time-Lapse Experiments. FhuA (− Fc) was injected (1 μM) over TonB proteins, (∼50 RU for TonB (FL) and ∼80 RU for TonB (CT)) and control surfaces for 20, 30, 60, or 240 s at 50 μL/min. After each FhuA injection regeneration was achieved with two pulses (10 s) of regeneration solution (5 mM NaOH, 0.1% Tween 20) followed by an EXTRACLEAN procedure performed according to the Biacore manual. Sensorgrams were then corrected by the double-referencing method (*25*). To facilitate the comparison between dissociation profiles of FhuA injected at different association times over TonB (FL), the response at the end of each association phase was normalized to an arbitrary value. Sensorgrams were then aligned so that the dissociation phase of the FhuA−TonB complexes began at 0 s on the *x*-coordinate. The same procedure was used for TonB (CT)−FhuA interactions.

Kinetic Characterization of TonB−FhuA Interactions by SPR. All kinetic experiments were carried out with a flow rate of 100 μL/min on CM4 or C1 sensor chips (Biacore, AB). Different concentrations of FhuA (in the absence of Fc or presence of 10 μM Fc; −/+ Fc) from 0 to 3000 nM were injected for 60 s over different TonB proteins; FhuA injections were randomly performed in triplicate. Analyte injections were then followed by buffer injection for 180 s. Between each FhuA injection regeneration of sensor chip surfaces was achieved by two 50 μL pulses of 5 mM NaOH, 0.1% Tween 20, followed by an EXTRACLEAN procedure.

Data were prepared using the double-referencing method (*25*) described by Khursigara et al. (*17*). All curves were reduced to 700 evenly spaced sampling points, and the initial 3 s of each curve were deleted prior to analysis (*25*). For each set of individual curves corresponding to injections of various concentrations of FhuA over the same TonB mutant surface kinetic analyses of the data were carried out using four kinetic models (simple, rearrangement, two-population, and avidity models) available in the SP*Revolution* software package (*26, 27*).

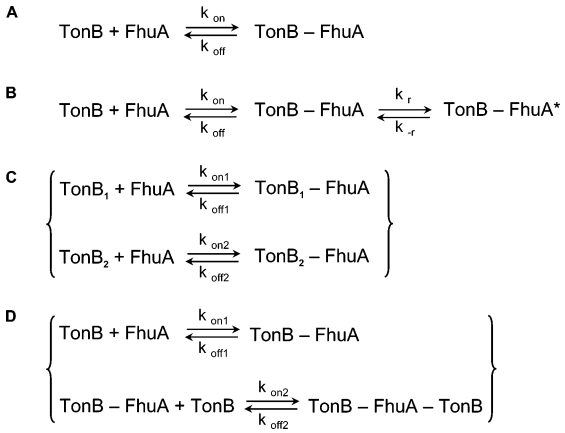

FIGURE 1: Schematic representation of the different kinetic models to describe TonB−FhuA interactions. For all models TonB represents the ligand (Biacore terminology) and FhuA the analyte. TonB−FhuA represents 1:1 complex, while TonB−FhuA−TonB represents 2:1 complex. Equation A depicts a simple Langmuirian interaction model. Equation B represents the rearrangement model where an initial TonB−FhuA complex undergoes a rearrangement to TonB−FhuA*. Equation C depicts the two-population model where two different populations TonB (i.e., $TonB_1$ and $TonB_2$) can bind to FhuA with different kinetic rates. Equation D represents the avidity model where a TonB−FhuA complex recruits a second TonB to form TonB −FhuA−TonB. For the rearrangement model K_d is defined as the thermodynamic constant related to the first step; $K_d = k_{off}/k_{on}$ (M). K_r corresponds to the thermodynamic constant related to the second step; $K_r = k_{-r}/k_r$ (no unit). The apparent K_d ($K_{d\,app}$) corresponding to ([TonB] × [FhuA])/([TonB − FhuA] + [TonB − FhuA*]) at equilibrium is equal to $[K_d^{-1} \times (1+ K_r^{-1})]^{-1}$. The apparent dissociation rate ($k_{off\,app}$) corresponds to ($K_{d\,app}$ x k_{on1}).

RESULTS

Our initial SPR experiments (*17*) examined interactions between TonB and FhuA using a random amine coupling approach for the immobilization of TonB proteins to the surface of the biosensor chips. With this coupling method attempts to analyze kinetics of TonB−FhuA interactions by SP*Revolution* did not provide an acceptable fit to a simple Langmuirian interaction model. Three models of varying complexity (Figure 1) equally well described data for TonB (FL)−FhuA interactions: a rearrangement model of initial complex formation followed by rearrangement to a more stable complex; a two-population model of two different populations of immobilized TonB interacting with FhuA; and an avidity model of FhuA interacting with one TonB molecule on the surface followed by recruitment of another TonB. Because computer analyses were unable to discriminate between different kinetic models when TonB was randomly coupled to the CM4 sensor surface, alternate coupling procedures for TonB proteins were investigated.

To reduce experimental effects of surface heterogeneity attributed to the random amine coupling procedure, a strategy was designed to mimic in vivo orientation of TonB when anchored in the CM. Site-directed cysteine mutagenesis of TonB (FL) and TonB (CT) proteins incorporated a single cysteine into the N-terminal linker region provided in the pET28 vector. No endogenous cysteine is found in either TonB protein. Expression, purification, solubility, and stability were the same for the TonB−cysteine mutants when compared to their parent, nonmutagenized proteins (data not shown). Taking advantage of the engineered cysteine residue,

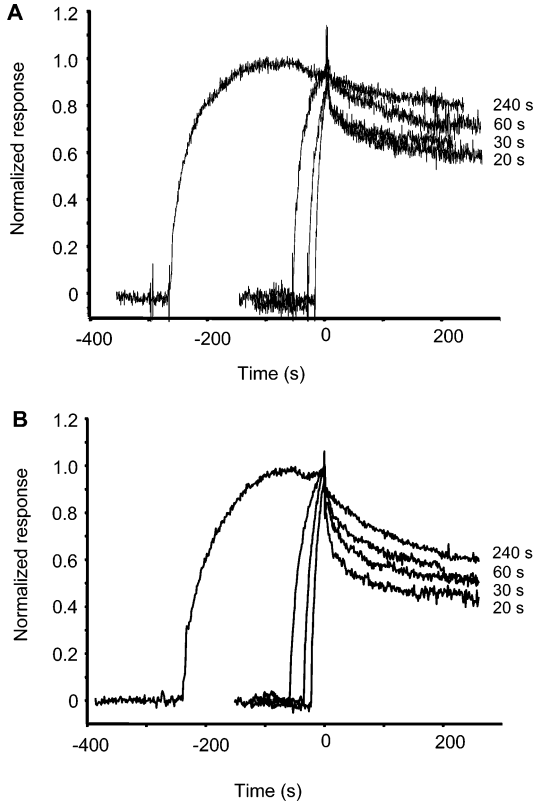

FIGURE 2: Time-lapse experiments for FhuA−Fc binding to TonB (FL) and TonB (CT). FhuA (1 μM) was injected at 50 μL/min for 20, 30, 60, and 240 s over TonB (FL) (A) and TonB (CT) (B). The sensorgrams were control-corrected and normalized at the end of each association phase to an arbitrary value. The beginning of the dissociation phase for each curve was aligned on the *x*-coordinate to zero in order to facilitate comparison of dissociation profiles.

thiol coupling of the purified TonB variants to the sensor chips created homogeneous TonB surfaces.

TonB−FhuA Interactions Are Comprised of Multiple Steps. To compare complexity of interactions for FhuA that were previously observed with amine-coupled TonB (FL) (*17*), time-lapse experiments were conducted with thiol-coupled TonB (FL). In the absence of Fc, FhuA (1 μM) was injected for association times varying between 20 and 240 s. If interactions between TonB and FhuA were to follow a simple Langmuirian association, the observed off rate should not change with respect to the duration of FhuA injections. However, if the interaction were comprised of multiple association steps, the observed off rate should vary with changes in association times. Figure 2A demonstrates the apparent dissociation of normalized FhuA injections over a TonB (FL) surface. As association times of FhuA were increased, the stability of the TonB (FL)−FhuA interactions also increased, as judged by slower dissociation profiles. This time-dependent phenomenon was also observed for TonB (CT)−FhuA interactions (Figure 2B), suggesting that FhuA interacted with both TonB species in a manner that deviated from a simple Langmuirian 1:1 interaction model. The deviation in dissociation profile was most evident at shorter association times (20, 30, and 60 s), indicating that the two-state mode of binding can be detected at shorter time intervals. The design of these experiments placed emphasis on low amounts of TonB coupled in an oriented fashion and on high flow rates. Therefore, the observed variation in dissociation cannot be attributed to nonoptimized experimental conditions, such as heterogeneity of the TonB surfaces due to random coupling (*28*). We hypothesized that the observed complexity results from a sequential multistep mechanism of interaction with a kinetically limiting element. On the basis of this observed time-dependent effect, FhuA injection times were set at 60 s over TonB surfaces for all subsequent kinetic experiments to fully assess the complexity of the initial interactions between TonB and FhuA.

Kinetic Assessment of Initial TonB (FL)−FhuA Interactions. Time-lapse experiments provided preliminary information about experimental parameters for subsequent detailed kinetic analyses. To further refine our kinetic experiments, flow rates were increased to 100 μL/min and low amounts of TonB protein were thiol-coupled, reducing surface heterogeneity, mass transport limitation, and rebinding artifacts (*29*). Furthermore, data sets were rigorously analyzed using the double-referencing method (*30*).

Interactions between thiol-coupled TonB (FL) and FhuA (−/+ Fc) were examined using CM4 sensor chips. We observed a marked decrease in the level of FhuA response in the presence of Fc (Figure 3B) as compared to the absence of Fc (Figure 3A). The difference at the highest FhuA concentration was approximately 2-fold. These trends were observed for all data generated by injecting the same FhuA concentrations (−/+ Fc) over similar TonB (FL) surfaces (data not shown). Given the complex mode of interaction observed in the time-lapse experiments, TonB (FL)−FhuA interactions were kinetically analyzed using a simple kinetic model. The nonrandom residuals and standard deviations demonstrate poor fits (Figure 3C and D). Because sources of artifact that might lead to deviation from a simple model were addressed by our experimental design, the observed deviations are consistent with a more complex mechanism of interaction between TonB (FL) and FhuA.

Our previous data demonstrated that in solution FhuA was capable of interacting with two TonB (FL) proteins by AUC, and a similar reduction in FhuA response over TonB (FL) surfaces was seen in steady-state SPR experiments (*17*). The decreased response level of bound FhuA observed upon Fc addition (Figure 3B) is likely due to an enhanced avidity effect occurring at the biosensor surface. That is, FhuA (+ Fc) might bind two TonB (FL) molecules in a more efficient fashion than the FhuA (− Fc) might bind two TonB (FL) molecules. Hence, less unbound TonB would be available to bind additional FhuA molecules at the surface of the biosensor, resulting in decreased response levels observed in the presence of Fc.

We next evaluated two kinetic models of higher complexity that describe the interactions: the rearrangement model and the avidity model (Figure 1B and D). Avidity describes binding strength of an interaction where one molecule contains multiple binding sites (multivalent), a term often invoked for antibody−antigen interactions. Within the SP*Revolution* software package the avidity model is used to analyze bivalent interactions because it depicts the presence of two independent binding sites on the analyte molecule (*31*). When used to analyze kinetics of TonB (FL)−FhuA interactions, these more complex models resulted in similar fits (Figure 3E−H), as judged by residuals (difference between experimental data and theoretical model) and their standard deviations. The same results were observed for three independently generated data sets over similar TonB (FL)

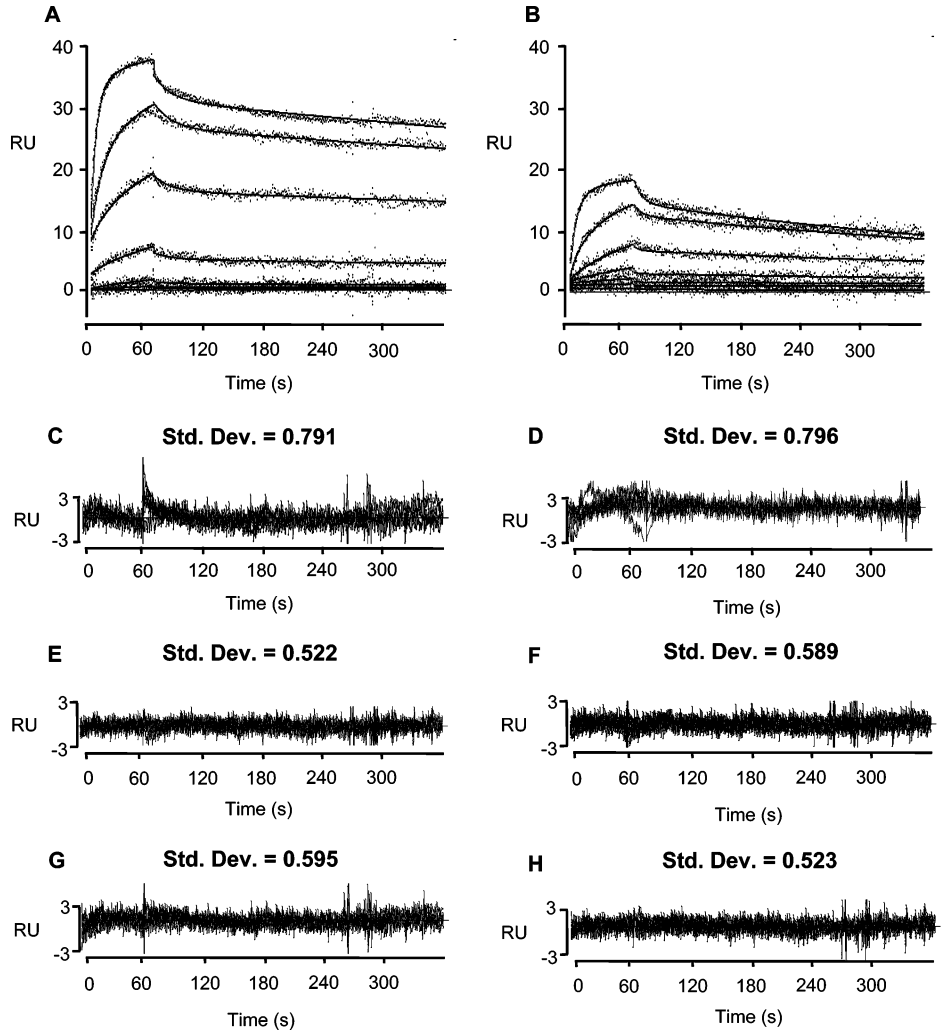

FIGURE 3: Kinetic analysis by SPR of FhuA interactions with TonB (FL) on CM4 sensor chip. Different concentrations (0, 10, 30, 100, 300, 1000, and 3000 nM) of FhuA − Fc (A) and FhuA + Fc (B) were injected in duplicate over 65 RUs of thiol-immobilized TonB (FL). The black points correspond to the experimental data and the solid lines to the fit using the rearrangement model in the case of FhuA − Fc and the avidity model in the case of FhuA + Fc. The kinetic and thermodynamic constants related to the fits are listed in Table 1. (C and D) Residuals for the fit to the simple model; (E and F) residuals for the fit to the rearrangement model; (G and H) fit to the avidity model for FhuA − Fc and FhuA + Fc, respectively. Standard deviations for each fit are listed above the respective residuals.

Table 1: Apparent Kinetic and Thermodynamic Constants of FhuA (−/+ Fc) Interacting with TonB (FL): Rearrangement Model[a]

	CM4 sensor chip		C1 sensor chip	
	FhuA (− Fc)	FhuA (+ Fc)	FhuA (− Fc)	FhuA (+ Fc)
$k_{on\ app}$ ($M^{-1}\ s^{-1}$)	$(27.3 \pm 1.0) \times 10^3$	$(27.3 \pm 1.0) \times 10^3$	$(31.6 \pm 1.0) \times 10^3$	$(30.4 \pm 1.0) \times 10^3$
$k_{off\ app}$ (s^{-1})	$(7.0 \pm 0.7) \times 10^{-4}$	$(3.1 \pm 1.0) \times 10^{-4}$	$(7.3 \pm 0.3) \times 10^{-4}$	$(7.6 \pm 0.5) \times 10^{-4}$
$K_{d\ app}$ (nM)	25.7 ± 3.0	11.5 ± 3.0	23.1 ± 2.7	25.0 ± 2.6

[a] Values correspond to average value ± the standard deviation of four independent experiments.

surfaces (data not shown). Similarities in the residuals associated with the more complex models did not allow us to discriminate between the fit of the rearrangement model versus the fit of the avidity model.

Muller et al. (*32*) proposed that description of the kinetic and thermodynamic parameters associated with the avidity effect are difficult to interpret. They demonstrated that the quality of fit obtained with an avidity model may be used to evaluate the adequacy of an interaction when compared to other models. However, the authors emphasized that the derived kinetics are less meaningful because the rates related to the second step of the avidity model are dependent on the amount of surface-bound protein. Acknowledging their caveats and then kinetically analyzing our data, only kinetic and thermodynamic constants for interactions of TonB (FL) with FhuA (−/+ Fc) with the rearrangement model are listed in Table 1. Despite best agreement between the experimental data and the avidity model in the case of FhuA (+ Fc) (Figure 3H; standard deviation = 0.523), kinetic rates determined for the avidity model have been omitted from our tables. Instead, the observed effect of Fc and its ability to promote stable 2:1 TonB (FL)−FhuA complexes is presented (Figure 3B).

To test the ability of TonB (FL) to dimerize upon addition of FhuA, we conducted additional experiments on C1 sensor chips. C1 sensor chips lack the flexible chains of carboxylated dextran that provide the three-dimensional matrix on CM4 sensor chips. Instead, the C1 surface is replaced by a

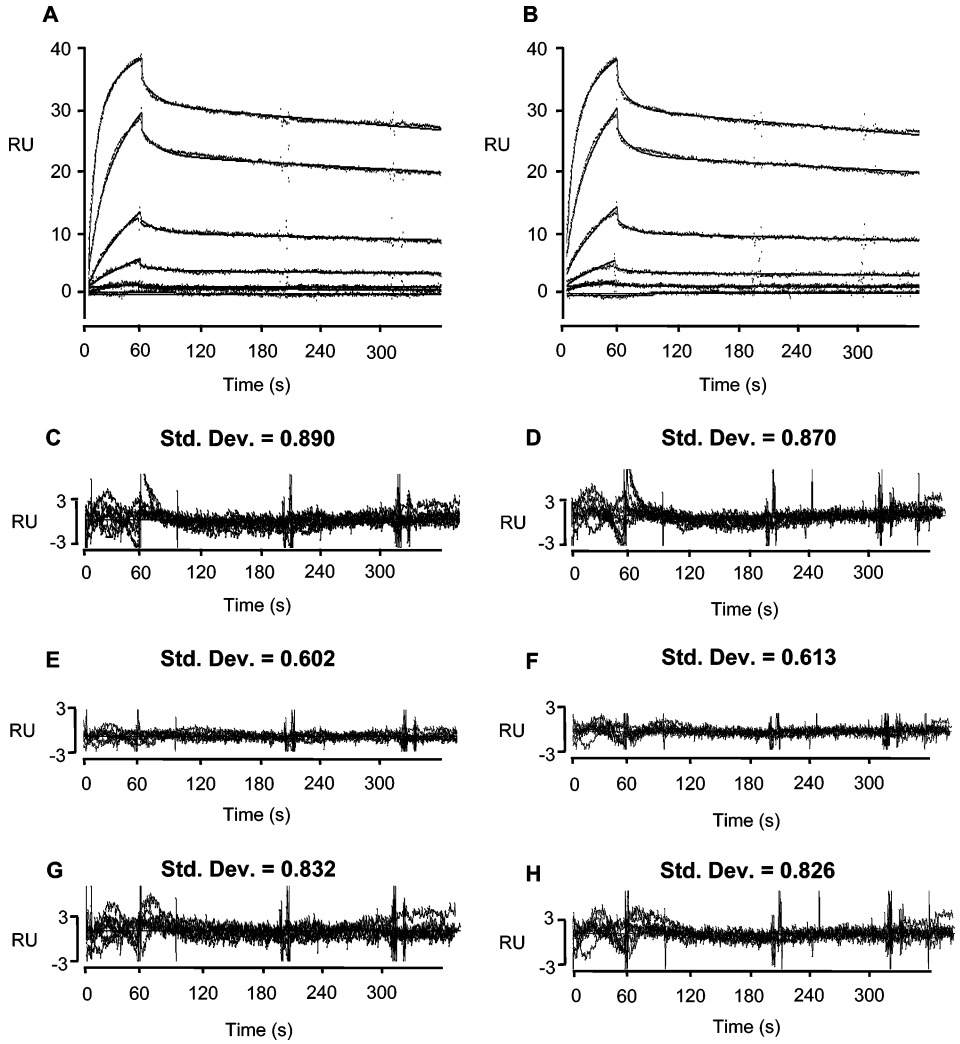

FIGURE 4: Kinetic analysis by SPR of FhuA interactions with TonB (FL) on C1 sensor chip. Different concentrations (0, 10, 30, 100, 300, 1000, and 3000 nM) of FhuA − Fc (A) and FhuA + Fc (B) were injected in duplicate over 118 RUs of thiol-immobilized TonB (FL) coupled to a C1 sensor chip. The black points correspond to the experimental data and the solid lines to the fit using the rearrangement model. The kinetic and thermodynamic constants related to the fits are listed in Table 1. (C and D) Residuals for the fit to the simple model; (E and F) residuals for the fit to the rearrangement model; (G and H) fit to the avidity model for FhuA − Fc and FhuA + Fc, respectively. Standard deviations for each fit are listed above the respective residuals.

flat two-dimensional carboxylated surface that supports the same immobilization chemistry. The absence of the dextran matrix reduces dynamic movement of immobilized proteins, thereby minimizing potential avidity effects (*33*). TonB (FL) was thiol coupled to the C1 chip (approximately 120 RU), and FhuA (−/+ Fc) was injected at different concentrations (0−3000 nM). As shown in Figure 4A and B, no apparent differences were observed in the levels of response or dissociation profile for FhuA (−/+ Fc) binding to TonB (FL).

Even though the avidity component was experimentally discounted, the interactions between TonB (FL) and FhuA were still not adequately described by a simple model (Figure 4C and D, − and + Fc, respectively) because of highest values for standard deviations. The complex interaction mechanism of binding was also highlighted by performing time-lapse experiments on the C1 chip, which provided similar dissociation profiles (data not shown) to those obtained with CM4 chips (Figure 2A). Analyses were extended by fitting the C1 sensor chip data using the rearrangement and the avidity models (Figure 4E−H). The rearrangement model was found to best describe the data rather than the avidity model, judging by residuals and standard deviations. Apparent kinetic and thermodynamic constants obtained when analyzing TonB (FL)−FhuA (−/+ Fc) interactions on C1 chips are listed in Table 1.

Our results from both CM4 and C1 sensor chips suggest that a kinetically limiting rearrangement of TonB (FL)−FhuA complex (1:1 stoichiometry) occurs prior to the recruitment of an additional TonB (FL) molecule. Apparent thermodynamic dissociation constants ($K_{d\ app}$) for TonB (FL)−FhuA interactions on a CM4 sensor chip demonstrated (Table 1) an increased affinity in the presence of Fc [$K_{d\ app}$; 25.7 (− Fc) versus 11.5 nM (+ Fc)]. Subsequent recruitment of a second TonB (FL) was enhanced by preincubation of Fc with FhuA and lead to formation of a more stable complex [$k_{off\ app}$; 7.0×10^{-4} (− Fc) versus 3.1×10^{-4} s^{-1} (+ Fc)]. On C1 sensor chips, absence of the three-dimensional dextran surface did not allow TonB (FL) molecules to bind to FhuA in a 2:1 manner; therefore, no reduction in response of FhuA over the TonB (FL) surface was observed (compare Figures 3A and B with 4A and B). The resulting affinities were not affected by Fc [$K_{d\ app}$ 23.1 (− Fc) versus 25.0 nM (+ Fc)] nor was the overall stability of the complex [$k_{off\ app}$ 7.3×10^{-4} (− Fc) versus 7.6×10^{-4} s^{-1} (+ Fc)]. These results

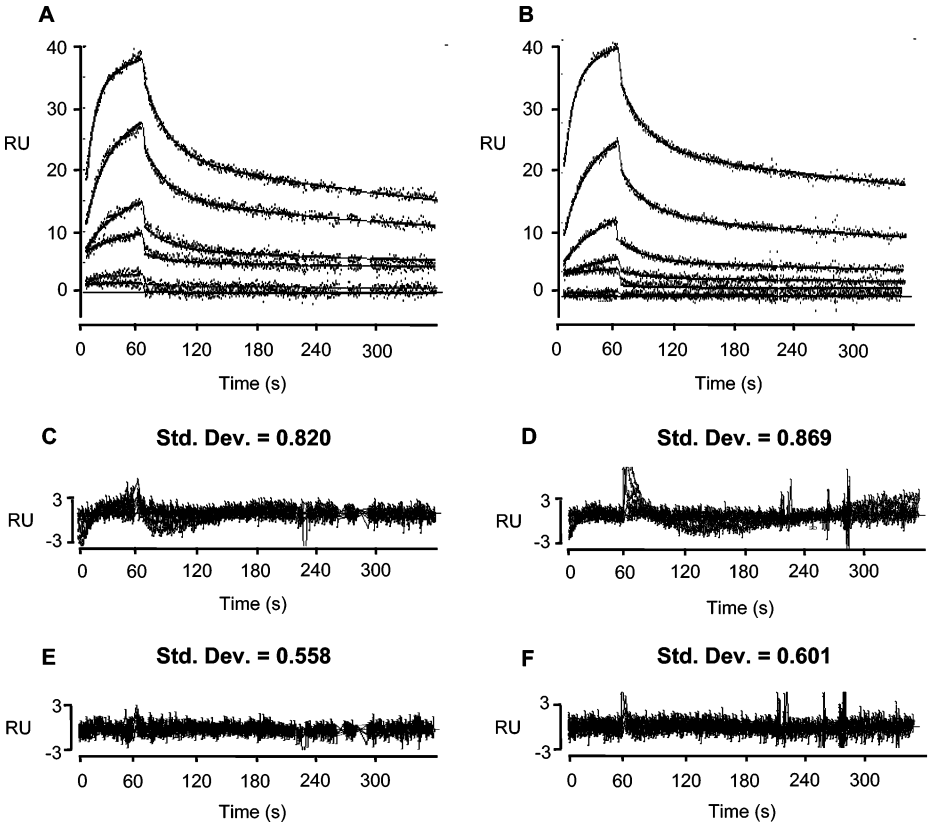

FIGURE 5: Kinetic analysis by SPR of FhuA interactions with TonB (CT). Different concentrations (0, 10, 30, 100, 300, 1000, and 3000 nM) of FhuA − Fc (A) and FhuA + Fc (B) were injected in duplicate over 61 RUs of thiol-immobilized TonB (CT). The black points correspond to the experimental data and the solid line to the fit using the rearrangement model for both FhuA − Fc and FhuA + Fc. The kinetic and thermodynamic constants related to the fits are listed in Table 2. (C and D) Residuals for the fit to the simple model; (E and F) fit to the rearrangement model for FhuA − Fc and FhuA + Fc, respectively. Standard deviations for each fit are listed above the respective residuals.

suggest that a kinetically limiting rearrangement governs initial interaction between TonB (FL) and FhuA; formation of a 2:1 TonB (FL)−FhuA complex follows.

Kinetic Assessment of Initial TonB (CT)−FhuA Interactions. TonB (CT) was shown to be a tightly intertwined dimer (*15*, *16*). When analyzed by steady-state SPR (*17*) this dimer was capable of binding to FhuA with reduced affinity when compared to TonB (FL). For kinetic analysis of TonB (CT)−FhuA interactions, approximately 60 RUs of TonB (CT) were thiol coupled to a CM4 sensor chip. Concentrations of FhuA (−/+ Fc) from 0 to 3000 nM were injected. In both the absence and presence of Fc (Figure 5A and B, respectively) the heights of each control-corrected sensorgram for matching FhuA concentrations were similar, indicating that Fc had no effect on the amount of FhuA binding to the immobilized TonB (CT) surface. As expected from time-lapse experiments, the interactions could not be adequately depicted by a simple model of binding (Figure 5C and D). We previously demonstrated by AUC that TonB (CT) was dimeric and bound to FhuA with a 2 TonB (CT):1 FhuA stoichiometry (*17*). The observed deviation from the simple model is likely due to each monomer within the TonB (CT) dimer interacting sequentially with FhuA. This mechanism of binding would correspond to the rearrangement model (Figure 1B). Thus, the control-corrected sensorgrams for FhuA (−/+ Fc) were fit to the rearrangement model (Figure 5E and F, respectively). As a control, the quality of the fit was compared to that obtained using the avidity model; both models are equally complex. The rearrangement model provided the best fit when compared to the avidity model (data not shown), consistent with previous observations that TonB (CT) exists as a preformed dimer (*16*, *17*). Kinetic and thermodynamic parameters corresponding to the TonB (CT)−FhuA interactions are listed in Table 2. A comparison of these constants revealed that preincubation of FhuA with Fc did not affect its interaction with TonB (CT). The apparent thermodynamic dissociation constants ($K_{d\,app}$) corresponding to FhuA interactions with TonB (CT) were higher [182.3 (− Fc) and 154.2 nM (+ Fc)] than for FhuA interactions with TonB (FL) [25.7 (− Fc) and 11.5 nM (+ Fc)]. This indicates that the overall affinity of FhuA for TonB (CT) is not as high as for TonB (FL). Such findings are in agreement with our steady-state analysis (*17*) and confirm that the N-terminal portion of TonB (FL) actively participates in binding to FhuA.

Table 2: Apparent Kinetic and Thermodynamic Constants of FhuA (−/+ Fc) Interacting with TonB (CT): Rearrangement Model[a]

parameters	FhuA (− Fc)	FhuA (+ Fc)
$k_{on\,app}$ ($M^{-1}s^{-1}$)	$(28.3 \pm 0.8) \times 10^3$	$(24.8 \pm 0.6) \times 10^3$
$k_{off\,app}$ (s^{-1})	$(5.2 \pm 0.6) \times 10^{-3}$	$(3.8 \pm 0.4) \times 10^{-3}$
$K_{d\,app}$ (nM)	182.3 ± 15.0	154.2 ± 17.3

[a] For footnote definitions see Table 1.

Deletion within the Cork Domain of FhuA Alters Stoichiometry of TonB−FhuA Complex. Prior to high-resolution structures of FhuA by X-ray crystallography (*5*, *6*) we engineered the FhuAΔ21−128 protein (*20*) to define domains of FhuA−ligand interactions. By inspection of the FhuA crystal structures this deletion is located in the cork domain

Table 3: Sedimentation Velocity Parameters of TonB (FL)−FhuAΔ21−128 Complexes Determined by Fits to a Noninteracting Discrete Species Model

FhuAΔ21−128	TonB(FL)	Fc	*s*3	M_a3^a (Da)	$\Phi_{avg}{}^b$ (mL/g)	M_r3^c (Da)	c_{S3}/c_{tot} (%)	rmsd[d]
1	2	−	2.66	22,533	0.756	92,357	55	0.0079
1	2	+	2.82	22,949	0.756	94,053	41	0.0057

FhuAΔ21−128 and TonB (FL) were mixed in the molar ratios indicated in the presence or absence of ferricrocin. *s*3, M_b3, M_r3 = FhuAΔ21−128 + TonB (FL) complex. [a] Buoyant molecular mass determined from fit to noninteracting discrete species model (SEDFIT); [b] Weight-averaged apparent vbar of complex; [c] $M_r = M_b/(1 - \Phi)$; [d] rmsd = least-squares error of fit.

(residues 1−160), eliminating the switch helix (residues 24−29) but not deleting the Ton box (residues 7−11). We modified the original FhuAΔ21−128 construct to incorporate a hexahistidine tag at position 405, thereby facilitating its purification. This same FhuA mutant was characterized by Bonhivers et al. (*34*), and its stability was compared to FhuA. The authors demonstrated that FhuAΔ21−128 had some reduced stability resulting from loss of cork residues. Our biophysical characterization of FhuAΔ21−128 exploited AUC and SPR to examine this engineered FhuA cork deletion for interactions with TonB.

To investigate the stoichiometry of TonB (FL)−FhuAΔ21−128 we performed sedimentation velocity AUC experiments on TonB (FL) and FhuAΔ21−128 individually and in mixtures. The sedimentation parameters (*s* and M_b) for the individual species were used as prior knowledge in analyzing the sedimentation behavior of TonB (FL)−FhuAΔ21−128 complexes in the absence and presence of Fc. Experiments were performed in the detergent C8E4 using methods and analytical procedures described previously (*17*). Uncomplexed FhuAΔ21−128 (− Fc) sedimented as a single species with an *s* value of 3.04 and a buoyant molecular mass (M_b) of 15 712 Da: such a value corresponds to a M_r of 68 017 Da and reflects the loss of 107 residues in the FhuA cork domain. This is in agreement with the findings of Bonhivers et al. that demonstrated by SDS−PAGE and nondenaturing gels a shift in migration of recombinant FhuAΔ21−128 proportional to the loss of residues 21−128 in the FhuA cork domain (*34*). In the presence of Fc we found FhuAΔ21−128 to have an *s* value of 2.99 and a buoyant molecular mass of 15 665 Da. The c(S) analyses revealed that the frictional ratio (f/f_o) of FhuAΔ21−128 is 1.80 in the absence of Fc and 1.89 in the presence of Fc. These values differ only slightly from the frictional ratio of FhuA (f/f_o = 1.76) determined in our previous study (*17*). TonB (FL) with a single Cys substitution sedimented as two species: a monomer with an *s* value of 1.61 and a M_b of 7102 Da and a dimer with an *s* value of 1.58 and a M_b of 14 367 Da. The dimeric TonB (FL) species is of lower abundance, comprising approximately 30% of c_{tot}, with monomeric TonB comprising the remaining 70%. We previously showed TonB (FL) lacking this Cys substitution sediments with an *s* value of 1.40 and a M_b of 6989 Da (*17*). The lower abundance dimeric species may be due to the formation of intermolecular disulfide bridges between TonB (FL) monomers.

Using the sedimentation parameters of the uncomplexed species as prior knowledge we performed sedimentation velocity experiments on 2:1 molar mixtures of TonB (FL) and FhuAΔ21−128 in the absence and presence of Fc (Table 3). Absorbance data were fit to the noninteracting discrete species model of SEDFIT. Both in the absence and presence of Fc three sedimenting species were observed: uncomplexed FhuAΔ21−128 (*s*1), uncomplexed dimeric TonB (FL) (*s*2), and TonB (FL)−FhuAΔ21−128 complex (*s*3). In analyzing these data the *s* and M_b parameters of *s*1 and *s*2 were fixed at the values described above. In the absence of Fc *s*3 was observed to have an *s* value of 2.66 and a M_b of 22 533 Da. In the presence of Fc the *s* value of the complex increased to 2.82 while the M_b remained the same (22 949 Da; Table 3). The increase in *s* suggests alterations in the overall shape of *s*3 in the presence of Fc and is consistent with the Fc-dependent increase in *s* previously observed for the 2:1 TonB (FL)−FhuA complex (*17*). Also consistent with our previous study, the observed complex has an *s* value that is slightly lower than that of the uncomplexed FhuA species, likely due to the elongated nature of TonB (FL) (*17*). We observed that *s*3 accounted for 55% and 41% of c_{tot} in the absence and presence of Fc, respectively (Table 3). The remainder of c_{tot} in each case was comprised of both uncomplexed FhuAΔ21−128 and uncomplexed TonB (FL).

The M_b values of *s*3 in the absence and presence of Fc are equivalent to the sum of the M_b values of one molecule of TonB (FL) plus one molecule of FhuAΔ21−128. Using a weight-averaged apparent vbar of 0.756 we determined the molecular mass of the complex to be 92 357 and 94 053 Da in the absence and presence of Fc, respectively (Table 3). These values agree well with the sequence-predicted molecular mass of a 1:1 TonB−FhuAΔ21−128 complex (93 049 Da). We previously showed (*17*) that TonB (FL) and FhuA form a 2:1 complex both in the absence and presence of Fc. However, here we were unable to fit our sedimentation velocity data to a model describing a 2:1 TonB−FhuAΔ21−128 complex. SEDFIT analyses of these data revealed the presence of only a 1:1 complex with no detectable 2:1 complex in the absence or presence of Fc.

Deletion within Cork Domain of FhuA Does Not Alter Initial TonB (FL)−FhuA Interactions. Interactions between TonB (FL) and FhuAΔ21−128 were analyzed by thiol coupling approximately 80 RUs of TonB (FL) to a CM4 sensor chip. Concentrations up to 3000 nM FhuA (−/+ Fc) were injected over test surfaces and control surfaces. Absence of residues 21−128 of FhuA abolishes formation of a 2:1 TonB (FL)−FhuA complex and thus is not expected to lead to a Fc-enhanced avidity at the sensor chip surface. In either the absence or the presence of Fc FhuAΔ21−128 demonstrated similar levels of response (Figure 6A and B). This observation is strikingly different than that for TonB (FL)−FhuA (−/+ Fc) interactions (Figure 3A and B), indicating that Fc does not contribute an avidity effect to the same extent. Also, the absence or presence of Fc did not improve the quality of the fit to the simple model (Figure 6C and D). Data were next analyzed using the rearrangement (Figure 6E and F) and avidity models (data not shown); TonB (FL)−FhuAΔ21−128 interactions, both in the absence and presence

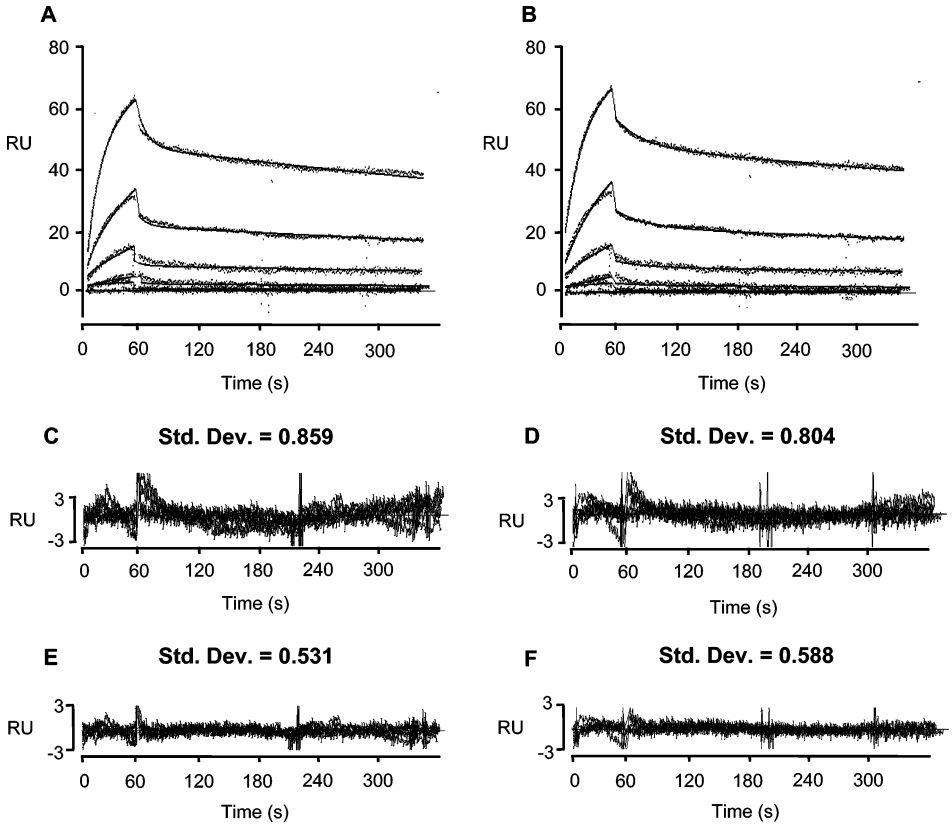

FIGURE 6: Kinetic analysis by SPR of FhuAΔ21−128 interactions with coupled TonB (FL). Different concentrations (0, 10, 30, 100, 300, 1000, and 3000 nM) of FhuAΔ21−128 − Fc (A) and FhuAΔ21−128 + Fc (B) were injected in duplicate over 89 RUs of thiol-immobilized TonB (FL). The black points correspond to the experimental data and the solid line to the fit using the rearrangement model for both FhuAΔ21−128 − Fc and FhuAΔ21−128 + Fc. The kinetic and thermodynamic constants related to the fits are listed in Table 4. (C and D) Residuals for the fit to the simple model; (E and F) fit to the rearrangement model for FhuAΔ21−128 − Fc and FhuAΔ21−128 + Fc, respectively. Standard deviations for each fit are listed above the respective residuals.

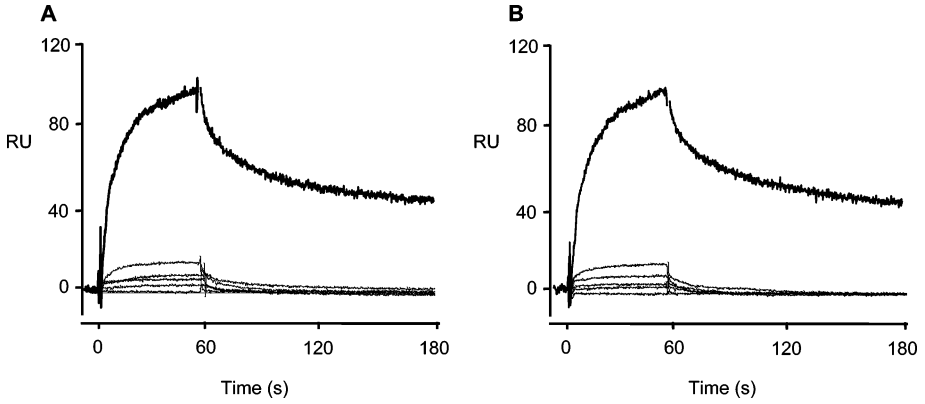

FIGURE 7: Evaluation of by SPR of FhuAΔ21−128 interactions with TonB (CT). Different concentrations (0, 100, 300, 1000 and 3000 nM) of FhuAΔ21−128 −Fc (panel A) and FhuAΔ21−128 +Fc (panel B) were injected in duplicate over 159 RUs of thiol-immobilized TonB (CT). The top curve (grey) in both panels A and B represent the surface-normalized response from FhuA − TonB (CT) interactions, − and + Fc respectively (Figure 4 A and B) at the 3000 nM concentration injection. Experiments were performed at 25 °C and at a flow rate of 100 μl/min.

of Fc, were best described by the rearrangement model as judged by residuals and standard deviations.

The kinetic and thermodynamic constants for TonB (FL)−FhuAΔ21−128 interactions as described by the rearrangement model are presented in Table 4. The overall affinity of the interaction [$K_{d\,app}$ = 20.1 (− Fc) versus 64.1 nM (+ Fc)] and stability of the complex [$k_{off\,app}$ = 7.4 × 10^{-4} (− Fc) versus 1.9 × 10^{-3} s^{-1} (+ Fc)] are stronger in the absence of Fc. The Fc-dependent increase in $K_{d\,app}$ agrees with our AUC data which demonstrate a slightly lower abundance of TonB (FL)−FhuAΔ21−128 complex in the presence of Fc (Table 3). This suggests that when FhuAΔ21−128 is in a ligand-loaded state, the cork deletion in FhuA may perturb potential

Table 4: Apparent Kinetic and Thermodynamic Constants of FhuAΔ21−128 (−/+ Fc) Interacting with TonB (FL): Rearrangement Model[a]

parameters	FhuA (− Fc)	FhuA (+ Fc)
$k_{on\,app}$ ($M^{-1}s^{-1}$)	(37.0 ± 1.0) × 10^3	(29.0 ± 1.0) × 10^3
$k_{off\,app}$ (s^{-1})	(7.4 ± 0.6) × 10^{-4}	(1.9 ± 0.3) × 10^{-3}
$K_{d\,app}$ (nM)	20.1 ± 4.0	64.1 ± 5.2

[a] For footnote definitions see Table 1.

sites of TonB interaction or the mutated cork may undergo drastic conformational changes when the ligand Fc is present.

Deletion within Cork Domain of FhuA Eliminates TonB (CT)−FhuA Interactions. Initial attempts to analyze interactions between TonB (CT) and FhuAΔ21−128 employed 61 RUs of thiol-coupled TonB (CT) on the surface of a CM4 sensor chip. Concentrations of FhuAΔ21−128 (−/+ Fc) from 0 to 3000 nM injected over a surface with a similar loading of TonB (CT) failed to produce a significant response. To increase the response the amount of TonB (CT) coupled to the surface was increased to 159 RUs, and the same concentrations of FhuAΔ21−128 (−/+ Fc) were injected as for FhuA. Only the highest concentrations (3000, 1000, 300, and 100 nM −/+ Fc) provided reproducible and detectable signals (Figure 7A and B). At these concentrations of FhuAΔ21−128 the complexes formed with TonB (CT) were determined to be transient, as judged by their apparent fast dissociation rate. Also, no effect of Fc on the interactions was observed (Figure 7B); there was no change in the level of response. For comparison, data from 3000 nM concentrations of FhuA (−/+ Fc) injected over 61 RUs of TonB (CT) were normalized to the response expected over the 159 RU surface (Figure 7A and B, gray curves). The differences in the level of response, the amplitude of the association, and the resulting stability of the complex reveal negligible interactions between TonB (CT) and FhuAΔ21−128.

DISCUSSION

Our previous steady-state SPR analysis (*17*) confirmed that FhuA interactions with TonB (FL) were enhanced by the preincubation of FhuA with Fc, demonstrating a 7-fold increase in affinity in the presence of Fc. However, attempts to analyze kinetics of FhuA interactions with amine-coupled TonB (FL) were complicated by surface heterogeneity, an experimental artifact (*25*), and did not allow determination of kinetic constants to describe the interactions. In the present study we carefully optimized our SPR experimental conditions by oriented thiol coupling. Addition of a single cysteine residue in the N-terminal linker region of both TonB variants provided an alternate immobilization of TonBs, producing a homogeneous surface that mimics in vivo orientation. Using these surfaces our kinetic analysis indicates that ligand-loaded FhuA forms a complex 2-fold more stable than its ligand-unloaded counterpart [$k_{off\ app} = 7.0 \times 10^{-4}\ s^{-1}$ (− Fc) versus 3.1×10^{-4} (+ Fc); Table 1]. This Fc-dependent increase in stability is directly reflected in the apparent affinities [$K_{d\ app}$ = 25.7 (− Fc) versus 11.5 nM (+ Fc)] of TonB for FhuA −/+ Fc since the apparent association rates of the interactions were determined to be identical both in the presence or the absence of Fc (Table 1). The differences in $K_{d\ app}$ between our steady-state and kinetic analyses are attributed to two factors: the immobilization technique used to couple TonB (FL) (random amine coupling versus oriented thiol coupling) and the amount of TonB (FL) coupled to the surface (100 RUs in our previous study versus 65 RUs in the present study). The latter is consistent with measured affinity differences. Considering that FhuA binds to TonB (FL) according to an avidity model, it is likely that the apparent affinity of FhuA for surface-bound TonB (FL) increases while increasing the amount of coupled TonB. The higher amount of free TonB (FL) on the surface would favor the formation of a 2:1 TonB−FhuA complex. Time-lapse experiments for interactions of FhuA with thiol-coupled TonB (FL) and TonB (CT) demonstrated that the interactions are kinetically complex (Figure 2A and B). These results were corroborated by kinetic analyses of the SPR data corresponding to FhuA (−/+ Fc) interacting with both TonB variants.

The kinetic analysis of FhuA interactions with TonB (FL) immobilized at its N-terminus provides a clearer depiction of complex formation since TonB (FL) is now coupled in a more functionally relevant orientation. SPR experiments conducted on CM4 and C1 sensor chips (Figures 3 and 4, respectively) demonstrate that at least two distinct steps follow the formation of an initial TonB (FL)−FhuA complex: a rearrangement of the initial 1:1 TonB (FL)−FhuA complex and then recruitment of a second TonB (FL). The presence of Fc enhances the 2:1 TonB (FL)−FhuA complex when TonB (FL) is thiol coupled to the CM4 sensor chip surface (Figure 3B). TonB (FL) and FhuA can form a 2:1 complex in the absence of Fc but with decreased stability (*17*). This combination of kinetic steps resulted in experimental data that fit well to both the rearrangement and avidity models (Figure 3).

SPR experiments on C1 sensor chips corroborate the sequential nature of kinetic steps that occur between FhuA (−/+ Fc) and TonB (FL) (Figure 4). These experiments suggest that when monomeric TonB (FL) is immobilized on a two-dimensional surface, recruitment of an additional TonB (FL) molecule by a 1:1 TonB (FL)−FhuA complex is greatly diminished. A comparison of $k_{off\ app}$ values from CM4 and C1 sensor chips (Table 1) indicates that apparent off rates are similar for 2:1 and 1:1 TonB (FL)−FhuA interactions. From these values it is unclear whether the recruited TonB (FL) interacts directly with FhuA or with the initial TonB (FL) in the 1:1 complex. However, on the basis of on AUC results obtained for FhuAΔ21−128 (see below) and fits of TonB (FL)−FhuA interactions to the avidity model, our interpretation is that TonB (FL) recruited to a 1:1 TonB (FL)−FhuA complex interacts with FhuA; additional TonB−TonB interactions cannot be excluded. Kinetic analysis of the TonB (FL)−FhuA SPR data generated with C1 sensor chips indicates that the interaction is complex even though the avidity effect was not observed. This led to our hypothesis that the observed complexity was due to a kinetically limiting rearrangement occurring with the TonB (FL)−FhuA complex, consistent with a best fit of our data to the rearrangement model (Figure 4).

Further evidence for the presence of a kinetically limiting rearrangement step in formation of TonB (FL)−FhuA complex came from experiments conducted with FhuAΔ21−128 and TonB (FL) (Figure 6; Tables 3 and 4). AUC analysis of TonB (FL) plus FhuAΔ21−128 revealed that deletion of a significant portion of the FhuA cork domain abrogates in vitro assembly of 2:1 TonB−FhuA complex. With AUC experimental conditions used previously to detect 2:1 TonB−FhuA complex (*17*) we now establish that TonB (FL) can only form a 1:1 complex with FhuAΔ21−128. The complex is stable: sedimentation velocity data fit well to SEDFIT's noninteracting discrete species model. This is in agreement with SPR analyses that show the TonB−FhuAΔ21−128 complex to have approximately the same stability as the TonB−FhuA complex; both have equivalent $k_{off\ app}$ values in the absence of Fc. In the presence of Fc, however, the

stability of the TonB−FhuAΔ21−128 complex decreases approximately 2.5-fold, also reflected in a decrease in abundance of *s*3 upon addition of Fc to our AUC sample. We observe a concomitant Fc-dependent increase in the sedimentation coefficient of *s*3 (2.66−2.82), suggesting that the conformational changes that we proposed during the formation of the 2:1 TonB−FhuA encounter complex occur before recruitment of the second TonB molecule at the periplasmic face of the OM receptor. Our AUC results strongly support our SPR data in which an avidity model best describes the interaction of FhuA with TonB (FL) immobilized in a functionally relevant orientation. By using FhuAΔ21−128 we trapped the intermediate 1:1 complex formed prior to recruitment of a second TonB monomer, a necessary step in forming 2:1 complex. Evidence for this recruitment is clearly seen in the avidity effect in SPR experiments when TonB (FL) is immobilized to CM4 chips; this effect is enhanced when the OM receptor is in the ligand-loaded state. Since FhuAΔ21−128 cannot facilitate conformational changes necessary to render the TonB dimerization competent, we did not observe in our AUC experiments a significant increase in the abundance of TonB−FhuAΔ21−128 complex nor transition to a 2:1 complex when FhuAΔ21−128 is ligand loaded.

Moeck and Letellier (*35*) characterized interactions between a truncated TonB protein and FhuA. These in vitro interactions demonstrated that H6.′TonB formed complexes with FhuA in solution and when one partner was immobilized on Ni^{2+}-NTA agarose resin. Complex formation was enhanced in the presence of Fc, consistent with other qualitative in vitro and in vivo results demonstrating ligand-induced enhancement of TonB−OM receptor interactions (*12*, *35*−*39*). Characterization of TonB−FhuA interactions reported here represent detailed quantitative assessments of in vitro interactions using recombinant proteins, thus advancing previous studies.

In the case of TonB (CT), crystallographic structures (*15*, *16*) and AUC studies (*16*, *17*) demonstrated that the C-terminal portion of TonB forms an intertwined dimer. Our proposal that a predimerized TonB (CT) protein is coupled to the sensor chip surface is in excellent agreement with our SPR data and is best described by a rearrangement model (Figure 5 and Table 2). However, contrary to TonB (FL)−FhuA interactions, these results suggest that FhuA initially interacts with one chain of the TonB (CT) dimer and then rearranges to a more stable and higher affinity complex in which the second TonB (CT) chain also contacts FhuA. Kinetic and thermodynamic constants related to FhuA (−/+ Fc) interacting with TonB (CT) are similar, indicating that there is only modest Fc-dependent effect on TonB (CT)−FhuA complex formation. Koedding et al. suggested (*16*) that a similar dimeric TonB variant, TonB-86 (residues 153−239), is not an energetically favored oligomer of TonB. Hence, this rearrangement, although well described by fits to the model, is not considered to be biologically favored.

The inability of FhuAΔ21−128 to effectively interact with TonB (CT) in the SPR assays (Figure 7) suggests that the deleted cork residues are important sites of binding between C-terminal residues of TonB. Alternatively, positioning of the cork may be altered, abrogating stable interactions. In either case, the outcome delineates regions of interaction between predimerized TonB (CT) and the cork domain of FhuA. This also confirms the higher affinity binding site within the N-terminal region of TonB (FL). Although FhuAΔ21−128 cannot form a stable complex with TonB (CT), it interacts with TonB (FL) with a $K_{d\ app}$ of 20.1 nM (− Fc) in a stable fashion ($k_{off\ app} = 7.4 \times 10^{-4}\ s^{-1}$).

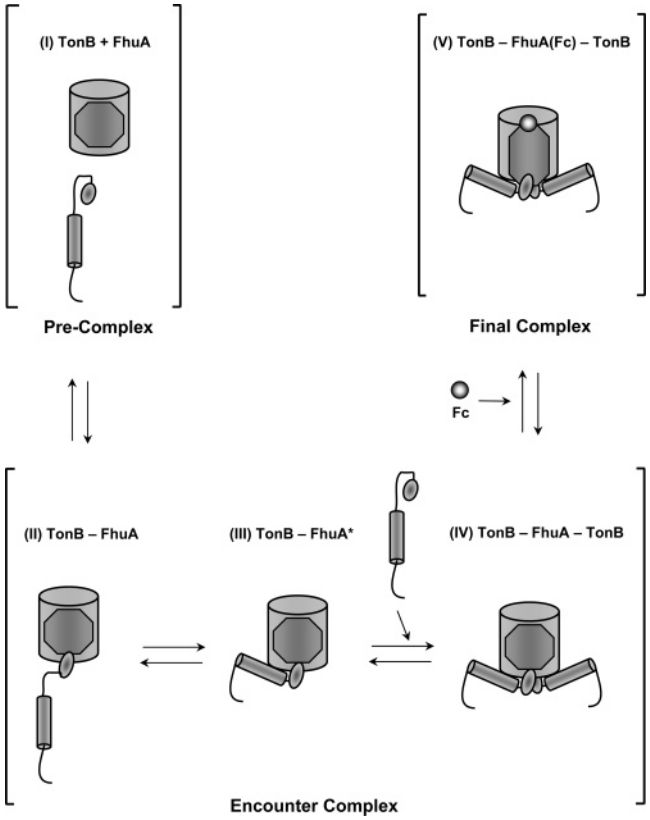

FIGURE 8: Proposed model of TonB−FhuA complex formation. The barrel shapes with the dark octagonal represent FhuA in the − Fc conformation. The oval shapes represent the C-terminal domain of TonB, which are connected to cylinders that represent the N-terminal binding region of TonB. The precomplex (I) consists of monomeric TonB (FL) and FhuA (− Fc). The encounter complex (II−IV) is comprised of an initial interaction mediated by the C-terminal portion of TonB (II) and a rearrangement to a higher affinity interaction mediated by an N-terminal portion of TonB (III). The rearrangement is followed by the recruitment of a second TonB (IV). The addition of Fc (shaded circle) enhances formation of the high-affinity 2:1 complex (V).

The initial rearrangement step of TonB (FL)−FhuA interactions is supported by studies demonstrating that the proton motive force and ligand-loaded OM-receptors can drive conformational changes in TonB (*36*). Mutations in aromatic residues within the C-terminus of TonB affect its ability to transport ligand due to altered conformational states (*40*). A related hypothesis has been proposed by Koedding et al.: TonB variants longer than 96 residues (from the C-terminus) contain secondary structure elements that promote an interaction between β-strands within the C-terminal region (*16*). This mechanism, by which TonB folds upon itself, was suggested to play a role in TonB−FhuA interactions, consistent with our observation that a rearrangement step occurs after the initial interaction between TonB (FL) and FhuA.

We now propose a detailed model for the mechanism of TonB−FhuA interactions (Figure 8). The precomplex stoichiometries (Step I) are comprised of monomeric TonB and monomeric FhuA. Step II is an initial interaction of a TonB

monomer with FhuA, characterized by low affinity and mediated by the C-terminus of TonB. On the basis of our results and other evidence this interaction most likely involves the Ton box of FhuA, although other sites of FhuA may participate in this interaction. Step III describes the rearrangement of the 1:1 TonB−FhuA complex to a higher affinity complex mediated by the N-terminal region of TonB. This rearrangement facilitates recruitment of a second TonB (Step IV); according to our AUC analysis this can occur in the absence of Fc. Importantly, Fc is required for formation of the high-affinity 2:1 TonB−FhuA complex (Step V), the most stable complex in all our experimental results. On the basis of results derived from the FhuAΔ21−128 mutant, we now propose that recruitment of two TonB monomers to FhuA requires the participation of the cork domain of OM receptors. However, all sites of interaction between TonB and OM receptors need to be more precisely identified, as do other sites of dimerization within TonB.

ACKNOWLEDGMENT

Canada Foundation for Innovation provided infrastructure for surface plasmon resonance to the Montreal Integrated Genomics Group for Research on Infectious Pathogens and for analytical ultracentrifugation to Hôpital Ste-Justine, Montreal. AUC support was from J.-C. Lavoie and L. Knafo, Montreal. Sheldon Biotechnology Centre is supported by a Multi-user Maintenance Grant from CIHR. P. Aliahmad and J.-N. Gagnon cloned several mutants. The authors thank M. O'Connor-McCourt and P. Schuck for insightful comments and J. A. Kashul for critical reading of the manuscript.

REFERENCES

1. Braun, V., Hantke, K., and Köster, W. (1998) in *Metal Ions in Biological Systems* (Sigel A and Sigael H, Eds.) pp 67−145, Marcel Dekker, Inc., New York.
2. Moeck, G. S., and Coulton, J. W. (1998) TonB-dependent iron acquisition: mechanisms of siderophore-mediated active transport, *Mol. Microbiol. 28*, 675−681.
3. Ferguson, A. D., Coulton, J. W., Diederichs, K., and Welte, W. (2001) in *Handbook of Metalloproteins* (Messerschmidt A., Huber, R., Poulos T., and Wieghardt K., Eds.) pp 834−849, John Wiley & Sons, Ltd., Chichester.
4. Postle, K., and Kadner, R. J. (2003) Touch and go: tying TonB to transport, *Mol. Microbiol. 49*, 869−882.
5. Ferguson, A. D., Hofmann, E., Coulton, J. W., Diederichs, K., and Welte, W. (1998) Siderophore-mediated iron transport: crystal structure of FhuA with bound lipopolysaccharide, *Science 282*, 2215−2220.
6. Locher, K. P., Rees, B., Koebnik, R., Mitschler, A., Moulinier, L., Rosenbusch, J. P., and Moras, D. (1998) Transmembrane signaling across the ligand-gated FhuA receptor: crystal structures of free and ferrichrome-bound states reveal allosteric changes, *Cell 95*, 771−778.
7. Buchanan, S. K., Smith, B. S., Venkatramani, L., Xia, D., Esser, L., Palnitkar, M., Chakraborty, R., van der Helm, D., and Deisenhofer, J. (1999) Crystal structure of the outer membrane active transporter FepA from *Escherichia coli*, *Nat. Struct. Biol. 6*, 56−63.
8. Ferguson, A. D., Chakraborty, R., Smith, B. S., Esser, L., van der Helm, D., and Deisenhofer, J. (2002) Structural basis of gating by the outer membrane transporter FecA, *Science 295*, 1715−1719.
9. Chimento, D. P., Mohanty, A. K., Kadner, R. J., and Wiener, M. C. (2003) Substrate-induced transmembrane signaling in the cobalamin transporter BtuB, *Nat. Struct. Biol. 10*, 394−401.
10. Skare, J. T., Ahmer, B. M., Seachord, C. L., Darveau, R. P., and Postle, K. (1993) Energy transduction between membranes. TonB, a cytoplasmic membrane protein, can be chemically cross-linked in vivo to the outer membrane receptor FepA, *J. Biol. Chem. 268*, 16302−16308.
11. Cadieux, N., and Kadner, R. J. (1999) Site-directed disulfide bonding reveals an interaction site between energy-coupling protein TonB and BtuB, the outer membrane cobalamin transporter, *Proc. Natl. Acad. Sci. U.S.A. 96*, 10673−10678.
12. Moeck, G. S., Coulton, J. W., and Postle, K. (1997) Cell envelope signaling in *Escherichia coli*. Ligand binding to the ferrichrome-iron receptor FhuA promotes interaction with the energy-transducing protein TonB, *J. Biol. Chem. 272*, 28391−28397.
13. Ogierman, M., and Braun, V. (2003) Interactions between the outer membrane ferric citrate transporter FecA and TonB: studies of the FecA TonB box, *J. Bacteriol. 185*, 1870−1885.
14. Günter, K., and Braun, V. (1990) In vivo evidence for FhuA outer membrane receptor interaction with the TonB inner membrane protein of *Escherichia coli*, *FEBS Lett. 274*, 85−88.
15. Chang, C., Mooser, A., Plückthun, A., and Wlodawer, A. (2001) Crystal structure of the dimeric C-terminal domain of TonB reveals a novel fold, *J. Biol. Chem. 276*, 27535−27540.
16. Koedding, J., Howard, P., Kaufmann, L., Polzer, P., Lustig, A., and Welte, W. (2004) Dimerization of TonB is not essential for its binding to the outer membrane siderophore receptor FhuA of *Escherichia coli*, *J. Biol. Chem. 279*, 9978−9986.
17. Khursigara, C. M., De Crescenzo, G., Pawelek, P. D., and Coulton, J. W. (2004) Enhanced binding of TonB to a ligand-loaded outer membrane receptor: role of the oligomeric state of TonB in formation of a functional FhuA·TonB complex, *J. Biol. Chem. 279*, 7405−7412.
18. Sauter, A., Howard, S. P., and Braun, V. (2003) In vivo evidence for TonB dimerization, *J. Bacteriol. 185*, 5747−5754.
19. Ferguson, A. D., Breed, J., Diederichs, K., Welte, W., and Coulton, J. W. (1998) An internal affinity-tag for purification and crystallization of the siderophore receptor FhuA, integral outer membrane protein from *Escherichia coli* K-12, *Protein Sci. 7*, 1636−1638.
20. Carmel, G., and Coulton, J. W. (1991) Internal deletions in the FhuA receptor of *Escherichia coli* K-12 define domains of ligand interactions, *J. Bacteriol. 173*, 4394−4403.
21. Moeck, G. S., Tawa, P., Xiang, H., Ismail, A. A., Turnbull, J. L., and Coulton, J. W. (1996) Ligand-induced conformational change in the ferrichrome-iron receptor of *Escherichia coli* K-12, *Mol. Microbiol. 22*, 459−471.
22. Moeck, G. S., Bazzaz, B. S., Gras, M. F., Ravi, T. S., Ratcliffe, M. J., and Coulton, J. W. (1994) Genetic insertion and exposure of a reporter epitope in the ferrichrome-iron receptor of *Escherichia coli* K-12, *J. Bacteriol. 176*, 4250−4259.
23. Schuck, P. (2000) Size-distribution analysis of macromolecules by sedimentation velocity ultracentrifugation and Lamm equation modeling, *Biophys. J. 78*, 1606−1619.
24. Johnsson, B., Lofas, S., and Lindquist, G. (1991) Immobilization of proteins to a carboxymethyldextran-modified gold surface for biospecific interaction analysis in surface plasmon resonance sensors, *Anal. Biochem. 198*, 268−277.
25. Rich, R. L., and Myszka, D. G. (2000) Advances in surface plasmon resonance biosensor analysis, *Curr. Opin. Biotechnol. 11*, 54−61.
26. De Crescenzo, G., Grothe, S., Zwaagstra, J., Tsang, M., and O'Connor-McCourt, M. D. (2001) Real-time monitoring of the interactions of transforming growth factor-beta (TGF-beta) isoforms with latency-associated protein and the ectodomains of the TGF-beta type II and III receptors reveals different kinetic models and stoichiometries of binding, *J. Biol. Chem. 276*, 29632−29643.
27. De Crescenzo, G., Grothe, S., Lortie, R., Debanne, M. T., and O'Connor-McCourt, M. (2000) Real-time kinetic studies on the interaction of transforming growth factor alpha with the epidermal growth factor receptor extracellular domain reveal a conformational change model, *Biochemistry 39*, 9466−9476.
28. O'Shannessy, D. J., and Winzor, D. J. (1996) Interpretation of deviations from pseudo-first-order kinetic behavior in the characterization of ligand binding by biosensor technology, *Anal. Biochem. 236*, 275−283.
29. Myszka, D. G. (1999) Improving biosensor analysis, *J. Mol. Recognit. 12*, 279−284.
30. Myszka, D. G. (1997) Kinetic analysis of macromolecular interactions using surface plasmon resonance biosensors, *Curr. Opin. Biotechnol. 8*, 50−57.
31. De Crescenzo, G., Pham, P. L., Durocher, Y., and O'Connor-McCourt, M. D. (2003) Transforming growth factor-beta (TGF-

beta) binding to the extracellular domain of the type II TGF-beta receptor: receptor capture on a biosensor surface using a new coiled-coil capture system demonstrates that avidity contributes significantly to high affinity binding, *J. Mol. Biol. 328*, 1173−1183.
32. Müller, K. M., Arndt, K. M., and Plückthun, A. (1998) Model and simulation of multivalent binding to fixed ligands, *Anal. Biochem. 261*, 149−158.
33. Walsh, S. T., Jevitts, L. M., Sylvester, J. E., and Kossiakoff, A. A. (2003) Site2 binding energetics of the regulatory step of growth hormone-induced receptor homodimerization, *Protein Sci. 12*, 1960−1970.
34. Bonhivers, M., Desmadril, M., Moeck, G. S., Boulanger, P., Colomer-Pallas, A., and Letellier, L. (2001) Stability studies of FhuA, a two-domain outer membrane protein from *Escherichia coli*, *Biochemistry 40*, 2606−2613.
35. Moeck, G. S., and Letellier, L. (2001) Characterization of in vitro interactions between a truncated TonB protein from *Escherichia coli* and the outer membrane receptors FhuA and FepA, *J. Bacteriol. 183*, 2755−2764.
36. Larsen, R. A., Thomas, M. G., and Postle, K. (1999) Protonmotive force, ExbB and ligand-bound FepA drive conformational changes in TonB, *Mol. Microbiol. 31*, 1809−1824.
37. Larsen, R. A., Foster-Hartnett, D., McIntosh, M. A., and Postle, K. (1997) Regions of *Escherichia coli* TonB and FepA proteins essential for in vivo physical interactions, *J. Bacteriol. 179*, 3213−3221.
38. Fanucci, G. E., Coggshall, K. A., Cadieux, N., Kim, M., Kadner, R. J., and Cafiso, D. S. (2003) Substrate-induced conformational changes of the periplasmic N-terminus of an outer-membrane transporter by site-directed spin labeling, *Biochemistry 42*, 1391−1400.
39. Merianos, H. J., Cadieux, N., Lin, C. H., Kadner, R. J., and Cafiso, D. S. (2000) Substrate-induced exposure of an energy-coupling motif of a membrane transporter, *Nat. Struct. Biol. 7*, 205−209.
40. Ghosh, J., and Postle, K. (2004) Evidence for dynamic clustering of carboxy-terminal aromatic amino acids in TonB-dependent energy transduction, *Mol. Microbiol. 51*, 203-213.

BI047882P